

# Measuring linear electric quadrupole susceptibility of non-centrosymmetric crystals with reflectivity difference EP

Cite as: Rev. Sci. Instrum. **92**, 025103 (2021); <https://doi.org/10.1063/5.0020686>

Submitted: 02 July 2020 . Accepted: 07 January 2021 . Published Online: 05 February 2021

 X. D. Zhu

## COLLECTIONS

EP This paper was selected as an Editor's Pick



View Online



Export Citation



CrossMark



**New**

## Your Qubits. Measured.

Meet the next generation of quantum analyzers

- Readout for up to 64 qubits
- Operation at up to 8.5 GHz, mixer-calibration-free
- Signal optimization with minimal latency

[Find out more](#)



Zurich Instruments

# Measuring linear electric quadrupole susceptibility of non-centrosymmetric crystals with reflectivity difference

Cite as: Rev. Sci. Instrum. 92, 025103 (2021); doi: 10.1063/5.0020686  
Submitted: 2 July 2020 • Accepted: 7 January 2021 •  
Published Online: 5 February 2021



X. D. Zhu<sup>a1</sup> 

## AFFILIATIONS

Department of Physics, University of California, Davis, California 95616, USA and Department of Optical Sciences and Engineering, Fudan University, Shanghai 200045, China

<sup>a1</sup>Author to whom correspondence should be addressed: [xdzhu@physics.ucdavis.edu](mailto:xdzhu@physics.ucdavis.edu)

## ABSTRACT

I report experimental methods for measuring real and imaginary parts of the linear electric quadrupole susceptibility tensor of nonlinear optical crystals that lack inversion centers. The third-ranked tensor is related to the corresponding second-order nonlinear susceptibility tensor. For opaque materials such as GaAs, the methods involve normal-incidence reflectivity difference detection schemes. For transparent materials, quadrupole susceptibility tensor elements may be measured with similarly construed transmission difference detection schemes.

Published under license by AIP Publishing. <https://doi.org/10.1063/5.0020686>

## I. INTRODUCTION

An atomic arrangement in a crystalline solid determines the symmetry group (point group) it belongs to. When the crystal is subject to external fields, responses to the fields and their gradients reveal the symmetry group. It is well-known that higher-order responses to external fields and their gradients can yield more information on the structural property of the crystal. When the external field is an electromagnetic wave, the lowest “high-order” process is the quadrupole response to the electric field gradient.<sup>1,2</sup> As a result, a linear polarization exists in response to the field gradient through a third-ranked tensor—electric quadrupole susceptibility tensor. Such a tensor has the same symmetry property as the second-order nonlinear susceptibility tensor<sup>3</sup> so that it has non-zero elements only in crystals that lack inversion centers, namely, in non-centrosymmetric crystals (a.k.a. nonlinear crystals). Zhu *et al.* recently demonstrated the existence of such a linear quadrupole response in GaAs.<sup>2</sup>

There are two useful applications of measuring linear quadrupole responses: (1) studying structural properties and phase transitions in some crystals with linear optics;<sup>4–7</sup> (2) characterizing the second-order nonlinearity of a nonlinear optical crystal.<sup>8</sup> Yet, experimental measurements of linear quadrupole responses have challenges. The first is that a detection scheme often only measures part of a susceptibility element, such as the real or the imaginary

part, or a particular combination of the two.<sup>2</sup> The second is that most nonlinear crystals have much smaller second-order nonlinearity than GaAs does.<sup>8</sup> In addition, third-ranked tensor elements in some of these materials are such that only at oblique incidence, they reveal symmetry properties of the crystals. Both lead to a much weaker effect on optical reflection. In this work, I show that a combination of reflectivity difference detection schemes can be used to separately measure the real part, the imaginary part, and the absolute amplitude of a quadrupole susceptibility tensor element of a nonlinear crystal such as GaAs. Similar schemes in the transmission geometry may be used to measure quadrupole susceptibility tensor elements in transparent nonlinear crystals.

## II. SYMMETRY PROPERTIES OF LINEAR ELECTRIC QUADRUPOLE RESPONSE IN NONLINEAR CRYSTALS

Unlike the electric dipole response in a material in which an induced electric polarization is a linear function of the electric field through a second-ranked tensor, a polarization arising from the quadrupole response is a linear function of the electric field gradient through a third-ranked tensor,

$$\vec{P}_Q^{(1)} = \epsilon_0 \vec{\chi}_Q^{(1)} : \nabla \vec{E} \quad (1)$$

or  $P_{Q,\alpha}^{(1)} = \epsilon_0 \chi_{EQ,\alpha\beta\gamma}^{(2)} : \nabla_\beta E_\gamma$ . It is useful to note that the second-order nonlinear dipole response is a quadratic function of the electric field through a third-ranked susceptibility tensor as well,

$$\vec{P}_D^{(2)} = \epsilon_0 \vec{\chi}_D^{(2)} : \vec{E}\vec{E}. \quad (2)$$

Both  $\vec{\chi}_Q^{(1)}$  and  $\vec{\chi}_D^{(2)}$  vanish in materials with inversion centers. For nonlinear optical crystals, susceptibility elements for both tensors have the same symmetry properties and are known in the literature.<sup>8</sup> It is easy to show that roughly  $\vec{\chi}_D^{(2)} \cong (e/\hbar\omega) \vec{\chi}_Q^{(1)}$ .<sup>3</sup> By measuring one of the two, we may estimate the other as an approximation.

Consider GaAs for an example. It belongs to the  $T_d$  or  $\bar{4}3m$  group. In the principal coordinate frame, only 6 out of 27 elements in  $\vec{\chi}_Q^{(1)}$  are non-zero, and they are equal in magnitude:  $\chi_{Q,xyz}^{(1)} = \chi_{Q,xzy}^{(1)} = \chi_{Q,yzx}^{(1)} = \chi_{Q,yxz}^{(1)} = \chi_{Q,zxy}^{(1)} = \chi_{Q,zyx}^{(1)} \equiv d_{14}$ .<sup>3</sup> In the visible range, GaAs is opaque, and thus,  $d_{14}$  has both a real part and an imaginary part. Inside the crystal, the gradient of the electric field mainly comes from the spatial variation of the phase, and Eq. (1) becomes<sup>1,2</sup>

$$\vec{P}_Q^{(1)} = \epsilon_0 (i \vec{\chi}_Q^{(1)} : \vec{k}) : \vec{E} = \epsilon_0 \Delta \vec{\epsilon}_Q : \vec{E}, \quad (3)$$

$$\Delta \vec{\epsilon}_Q = i \vec{\chi}_{EQ} : \vec{k}. \quad (4)$$

$\Delta \vec{\epsilon}_Q$  is the effective change in the dielectric tensor due to the electric quadrupole response.  $\vec{k}$  is the wave vector of the electromagnetic wave in the crystal. When expressed in the principal coordinate frame, I have

$$\Delta \vec{\epsilon}_Q = id_{14} \begin{pmatrix} 0 & k_z & k_y \\ k_z & 0 & k_x \\ k_y & k_x & 0 \end{pmatrix}. \quad (5)$$

$\Delta \vec{\epsilon}_Q$  has a different form when the laboratory coordinate frame does not overlap with the principal frame. To a degree, the transformation of  $\Delta \vec{\epsilon}_Q$  reveals the crystalline symmetry. Let the two coordinate frames overlap initially. When the principal frame rotates about the common  $z$  axis counter-clockwise by angle  $\phi$ , in the laboratory frame, I now have

$$\Delta \vec{\epsilon}_Q(\phi) = id_{14} \begin{pmatrix} k_z \sin 2\phi & k_z \cos 2\phi & k_x \sin 2\phi \\ k_z \cos 2\phi & -k_z \sin 2\phi & k_x \cos 2\phi \\ k_x \sin 2\phi & k_x \cos 2\phi & 0 \end{pmatrix}. \quad (6)$$

By experimentally measuring these tensor elements that exhibit distinct azimuth dependence, one can study structural properties and even phase transition in nonlinear crystals using linear optics.

### III. REFLECTIVITY DIFFERENCE MEASUREMENTS OF A LINEAR QUADRUPOLE SUSCEPTIBILITY TENSOR

$\Delta \vec{\epsilon}_Q(\phi)$  from a linear quadrupole response amounts to a small correction to the dielectric tensor. It produces small corrections to optical reflection and transmission and distinguishes itself through a characteristic azimuth dependence. Since  $\Delta \vec{\epsilon}_Q(\phi)$  cannot be modulated externally, one needs to use detection schemes that suppress the zeroth order reflection and transmission while keeping the

quadrupole effect more or less intact. For opaque crystals such as GaAs, one can only measure the correction to optical reflection. I next describe two reflectivity difference detection schemes for full  $\Delta \vec{\epsilon}_Q(\phi)$  characterization.

I start with a GaAs(001) surface with the  $z'$  axis of the principal frame pointing into the surface. The  $x$ - $y$ - $z$  axes of the laboratory coordinate frame initially overlap with  $x'$ - $y'$ - $z'$  axes of the principal coordinate frame. The principal frame is allowed to rotate about its  $z'$  axis (same as the laboratory  $z$  axis) counter-clockwise subsequently. The change in the linear dielectric tensor,  $\Delta \vec{\epsilon}_Q(\phi)$ , produces small corrections to the electric fields in reflection and modifies the reflection matrix  $R$  that relates  $s$ -polarized and  $p$ -polarized components of the reflected electric field to those of an incidence electric field. Let an optical beam incident from the ambient with  $\vec{e}_1 = \epsilon_1 \vec{I}$  at angle  $\theta_{inc}$  on the (001) surface of GaAs(001) with  $\vec{e}_2 = \epsilon_2 \vec{I} + \Delta \vec{\epsilon}_Q(\phi)$ . By choosing the  $x$ - $z$  plane as the incidence plane, the electric field of the incident beam is given by  $\vec{E}_1^{(+)} \exp(ik_{1x}^{(+)}x + ik_{1z}^{(+)}z)$ . The fields of the reflected and transmitted beams are written as  $\vec{E}_1^{(-)} \exp(ik_{1x}^{(-)}x - ik_{1z}^{(-)}z)$  and  $\vec{E}_2^{(+)} \exp(ik_{2x}^{(+)}x + ik_{2z}^{(+)}z) = \vec{E}_2^{(+)} \exp(ik_{1x}^{(+)}x + ik_{2z}^{(+)}z)$ , with  $k_{1x}^{(+)} = (2\pi/\lambda)\sqrt{\epsilon_1}\sin\theta_{inc}$ ,  $k_{1z}^{(+)} = (2\pi/\lambda)\sqrt{\epsilon_1}\cos\theta_{inc}$ , and  $k_{2z}^{(+)} = (2\pi/\lambda)\sqrt{\epsilon_2 - \epsilon_1\sin^2\theta_{inc}}$ . Figure 1 shows the laboratory frame and the convention of  $s$ -polarization and  $p$ -polarization for  $\vec{E}_1^{(+)}$ ,  $\vec{E}_1^{(-)}$ , and  $\vec{E}_2^{(+)}$ . The reflected electric field is related to the incident electric field through a reflection matrix,

$$\begin{pmatrix} E_{1p}^{(-)} \\ E_{1s}^{(-)} \end{pmatrix} = R \begin{pmatrix} E_{1p}^{(+)} \\ E_{1s}^{(+)} \end{pmatrix} = \left[ \begin{pmatrix} r_{pp}^{(0)} & 0 \\ 0 & r_{ss}^{(0)} \end{pmatrix} + \begin{pmatrix} \Delta r_{pp} & \Delta r_{ps} \\ \Delta r_{sp} & \Delta r_{ss} \end{pmatrix} \right] \begin{pmatrix} E_{1p}^{(+)} \\ E_{1s}^{(+)} \end{pmatrix}. \quad (7)$$

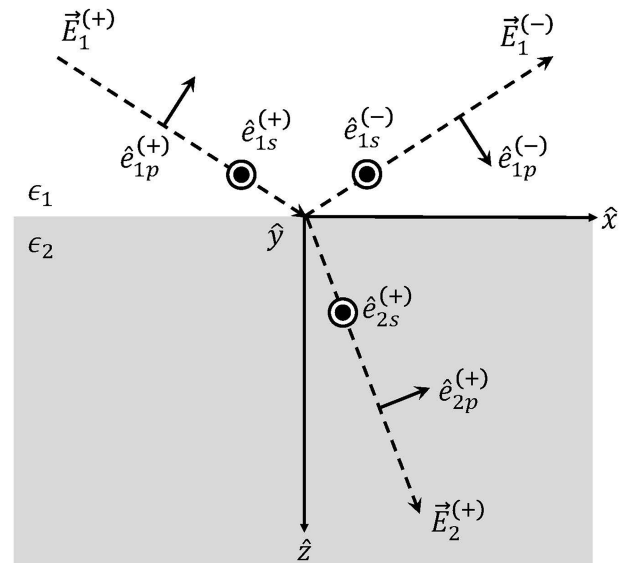


**FIG. 1.** The incident, reflected, and transmitted electric fields in the laboratory coordinate frame and choices of unit vectors for  $s$ -polarization and  $p$ -polarization are indicated.

$r_{pp}^{(0)}$  and  $r_{ss}^{(0)}$  are zeroth order reflection coefficients (reflectivities).  $\Delta r_{pp}$ ,  $\Delta r_{ps}$ ,  $\Delta r_{ps}$ , and  $\Delta r_{ss}$  are corrections due to  $\Delta \vec{\epsilon}_Q(\phi)$ . From Eq. (6), it is clear that some of the azimuth-dependent tensor elements in  $\Delta \vec{\epsilon}_Q(\phi)$  remain when  $\theta_{inc} = 0$ ,  $k_x = k_{2x}^{(+)} = k_{1x}^{(+)} = 0$ , and  $k_z = k_{2z}^{(+)} = (2\pi/\lambda)\sqrt{\epsilon_2}$ . As a result, at normal incidence, the correction to the reflection matrix becomes<sup>9</sup>

$$\begin{pmatrix} \Delta r_{pp} & \Delta r_{ps} \\ \Delta r_{sp} & \Delta r_{ss} \end{pmatrix} = \begin{pmatrix} -a \sin 2\phi & -a \cos 2\phi \\ -a \cos 2\phi & +a \sin 2\phi \end{pmatrix}, \quad (8)$$

with  $a = id_{14}(2\pi/\lambda) \frac{\sqrt{\epsilon_1}}{(\sqrt{\epsilon_1} + \sqrt{\epsilon_2})^2}$ . At normal incidence,  $r_{pp}^{(0)} = r_{ss}^{(0)} \equiv r_0$ . I can write the modified reflection matrix as follows:

$$R(\theta_{inc} = 0) = \begin{pmatrix} r_0 - a \sin 2\phi & -a \cos 2\phi \\ -a \cos 2\phi & r_0 + a \sin 2\phi \end{pmatrix}. \quad (9)$$

This means that for crystals such as GaAs, one can use normal-incidence reflectivity difference detection schemes on the (001) surface to measure linear quadrupole responses.

#### IV. EXPERIMENTAL PROCEDURES AND DATA PROCESSING

##### A. Normal-incidence detection scheme for measuring $Re\{a/r_0\}$

Figure 2 displays a detection scheme employed by Zhu *et al.* in the original study of the linear quadrupole response in GaAs.<sup>2</sup> In this scheme, a *p*-polarized He-Ne laser beam (0.5 mW and  $\lambda = 0.633 \mu\text{m}$ ) passes through a photo-elastic modulator (PEM-90, Hinds Instrument, Hillsboro, OR) with its fast axis at  $+45^\circ$  from the *p*-polarization. PEM-90 adds a time-varying phase  $\Phi(t) = \Phi_0 \cos(2\pi ft)$  between components along the slow axis and the fast axis of the modulator at  $f = 50$  kHz. The beam, then, passes through a phase shifter that adds an adjustable phase difference between the *p*-polarized and *s*-polarized components of the beam. It is a quarter-waveplate made of quartz with its fast axis along

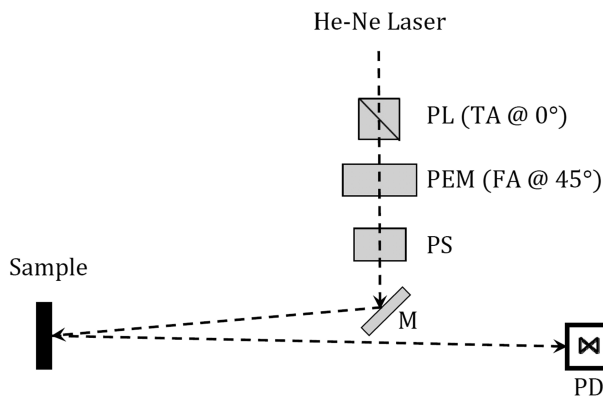


**FIG. 2.** Optical layout for a normal-incidence reflectivity difference detection scheme. A laser beam passes through a linear polarizer (PL), a photo-elastic modulator (PEM), and a phase shifter (PS) or phase compensator. After reflection of a bending mirror, it is incident on the sample near normal incidence. The reflected beam is detected with a photodetector (PD).

the horizontal direction. By rotating the waveplate about the vertical axis with a rotary stage, a variable phase difference is added between the *s*-polarized and *p*-polarized components of the passing beam. After a bending mirror, the beam is incident on the sample near normal incidence. The phase-sifter is used to compensate for the phase difference introduced by the bending mirror. The intensity of the reflected beam  $I(t)$  is detected with a Si photodiode (S2387-130R, Hamamatsu Corp., Bridgewater, NJ), followed by a home-built amplifier with a gain of  $5 \times 10^4$  V/A. The output from the amplifier is analyzed with two separate lock-in amplifiers (SR830, Stanford Research Systems, Sunnyvale, CA) to yield the first and second harmonics of the modulation frequency,  $I(f)$  and  $I(2f)$  in  $I(t)$ . From Eq. (A8) in the Appendix, by setting  $\Phi_p - \Phi_p + \Delta_{ps} = 90^\circ$ , they are given by the following expressions:

$$\begin{aligned} I(f) &= -4I_{inc}|r_0|^2 J_1(\Phi_0) Re\{\Delta r_{ps}/r_0\} \\ &= 4I_{inc}|r_0|^2 J_1(\Phi_0) Re\{a/r_0\} \cos 2\phi, \end{aligned} \quad (10)$$

$$\begin{aligned} I(2f) &= -4I_{inc}|r_0|^2 J_2(\Phi_0) Re\{\Delta r_{pp}/r_0\} \\ &= 4I_{inc}|r_0|^2 J_2(\Phi_0) Re\{a/r_0\} \sin 2\phi. \end{aligned} \quad (11)$$

In the earlier study,<sup>2</sup> Zhu *et al.* showed that Eqs. (10) and (11) indeed describe the observed azimuth dependence and confirmed the expected magnitude of the electric quadrupole effect. The advantage of this scheme is that it detects both off-diagonal ( $\Delta r_{ps}$ ) and diagonal ( $\Delta r_{pp}$ ) elements in the reflection matrix. The disadvantage is that it only measures the real part of  $a/r_0$ . This limitation is resolved in a different normal-incidence detection scheme as described next.

##### B. Normal-incidence detection scheme for measuring $Im\{a/r_0\}$ and $|a/r_0|$

Figure 3 shows a modified scheme for detecting the normal-incidence reflection difference. In this case, the initial He-Ne laser

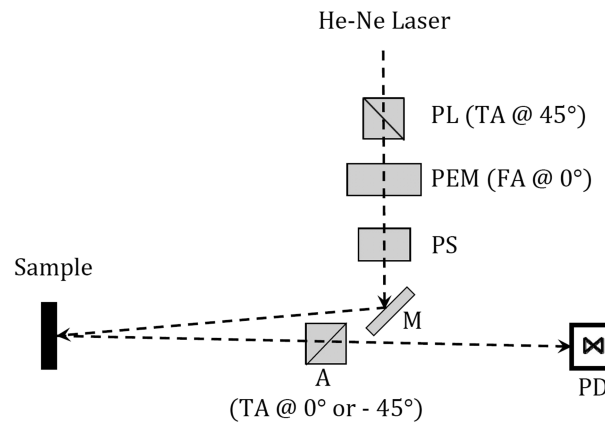


**FIG. 3.** Optical layout for another normal-incidence reflectivity difference detection scheme. In this case, the linear polarizer (PL) and the photoelastic modulator (PEM) are oriented differently from their configurations in Fig. 1. The reflected beam passes through an analyzing polarizer (A) before it is detected with the photodetector (PD).

beam (0.5 mW and  $\lambda = 0.633\mu\text{m}$ ) is linearly polarized along the direction  $+45^\circ$  from the  $p$ -polarization (the horizontal direction). It passes through a photoelastic modulator (PEM-90) with the fast axis now parallel to the  $p$ -polarization. The modulator adds a time-varying phase  $\Phi(t) = \Phi_0 \cos(2\pi ft)$  to the  $s$ -polarized component of the passing beam at  $f = 50$  kHz. In this work,  $\Phi_0 = \pi/2$ . The beam, then, passes through a phase shifter (PS) that adds an adjustable phase  $\Delta_{PS}$  between the  $p$ -polarized and  $s$ -polarized components, the same as the one in Fig. 2. After a bending mirror, the beam illuminates the sample near normal incidence. The phase shifter is used to compensate for phase differences introduced by the bending mirror and by the reflection matrix elements, namely, parameters  $a$  and  $r_0$  in Eq. (9). The reflected beam passes through an analyzing polarizer with its transmission axis (TA) at an angle  $\theta_A$  variable from the  $p$ -polarized component of the reflected beam. The analyzer serves to mix the  $s$ -polarized and  $p$ -polarized components of the reflected beam and enables detection of  $\text{Im}\{a/r_0\}$  and  $|a/r_0|$ . The beam intensity  $I(t)$  after the analyzer is detected with a combination of a Si photodiode (S2387-130R, Hamamatsu Corp., Bridgewater, NJ) and the home-built amplifier. The output of the amplifier is analyzed with two lock-in amplifiers (SR830, Stanford Research Systems, Sunnyvale, CA) to yield the first and second harmonics of the modulation frequency, i.e.,  $I(f)$  and  $I(2f)$ . According to Eq. (A14) in the Appendix,  $I(t)$  at the Si photodiode detector is expressed as follows:

$$I(t) = \frac{I_{inc}|r_0|^2}{2} + I_{inc}|r_0|^2 \sin \theta_A \cos \theta_A \times [\cos \Phi(t) \cos(\alpha - 2\gamma) + \sin \Phi(t) \sin(\alpha - 2\gamma)] - I_{inc}|r_0|^2 \left| \frac{a}{r_0} \right| \cos 2\phi [\cos^2 \theta_A \cos(\alpha - \beta - \Phi(t)) + \sin^2 \theta_A \cos(\alpha + \beta - \Phi(t))], \quad (12)$$

with  $\alpha \equiv \Phi_p - \Phi_s - \Delta_{PS}$ , where  $\Phi_p$  and  $\Phi_s$  are phase changes for  $p$ -polarized and  $s$ -polarized components of the beam due to reflection at the bending mirror.  $\beta = \arg\{a/r_0\}$ , and  $\gamma \equiv -\text{Im}\{\Delta r_{pp}/r_0\} = \text{Im}\{a/r_0\} \sin 2\phi$ .

By setting the TA of the analyzer to  $\theta_A = 0^\circ$ , I arrive at

$$I(f) = -2 * I_{inc}|r_0|^2 * J_1(\Phi_0) * |a/r_0| * \sin(\alpha - \beta) * \cos 2\phi, \quad (13)$$

$$I(2f) = +2 * I_{inc}|r_0|^2 * J_2(\Phi_0) * |a/r_0| * \cos(\alpha - \beta) * \cos 2\phi. \quad (14)$$

By adjusting the phase shifter, namely,  $\Delta_{PS}$ , to make either  $\alpha - \beta = 0$  or  $\alpha - \beta = 90^\circ$ , one of the harmonics vanishes and the other yields  $|a/r_0|$ . For example, with  $\alpha - \beta = 90^\circ$  so that  $I(2f) = 0$ , I have

$$I(f) = -2 * I_{inc}|r_0|^2 * J_1(\Phi_0) * |a/r_0| * \cos 2\phi. \quad (15)$$

By chopping the laser beam with a mechanical chopper at 1 kHz without changing any part in Fig. 3, I measure  $I_{inc}|r_0|^2$ . This allows the extraction of  $|a/r_0|$  completely.

By setting TA of the analyzer to  $\theta_A = -45^\circ$ , and further setting  $\alpha = 0^\circ$  to minimize  $I(f)$ , I have

$$I(f) = 2 * I_{inc}|r_0|^2 * J_1(\Phi_0) * \text{Im}\{a/r_0\} * \sin 2\phi, \quad (16)$$

$$I(2f) = I_{inc}|r_0|^2 * J_2(\Phi_0) * [1 + 2 * \text{Re}\{a/r_0\} * \cos 2\phi]. \quad (17)$$

$\text{Im}\{a/r_0\}$  is measured from  $I(f)$ .  $\text{Im}\{a/r_0\}$  can also be measured with  $I(2f)$  by setting  $\alpha = -90^\circ$  to minimize  $I(2f)$  initially. In this case,

$$I(f) = I_{inc}|r_0|^2 * J_1(\Phi_0) * [1 + 2 * \text{Re}\{a/r_0\} * \cos 2\phi], \quad (18)$$

$$I(2f) = -2 * I_{inc}|r_0|^2 * J_2(\Phi_0) * \text{Im}\{a/r_0\} * \sin 2\phi. \quad (19)$$

By separately measuring  $I_{inc}|r_0|^2$ ,  $\text{Im}\{a/r_0\}$  is obtained.

### C. Measuring the real part of $a/r_0$ ( $\text{Re}\{a/r_0\}$ ) with minor modification to Fig. 3

If the analyzer in Fig. 3 is removed, the  $s$ -polarized and  $p$ -polarized components of the reflected beam are no longer mixed before detection. As a result, the first and second harmonics become [see Eq. (A17) in the Appendix for details]

$$I(f) = -4 * I_{inc}|r_0|^2 * J_1(\Phi_0) * \text{Re}\{a/r_0\} * \sin \alpha * \cos 2\phi, \quad (20)$$

$$I(2f) = +4 * I_{inc}|r_0|^2 * J_2(\Phi_0) * \text{Re}\{a/r_0\} * \cos \alpha * \cos 2\phi. \quad (21)$$

Again with the separate measurement of  $I_{inc}|r_0|^2$  by chopping the laser beam with a mechanical chopper at 1 kHz,  $\text{Re}\{a/r_0\}$  is completely extracted.

## V. RESULTS AND DISCUSSION

### A. Measuring $|a/r_0|$

In Fig. 4, I show  $-I(f)/I_{inc}|r_0|^2$  as a function of  $\phi$  measured from a GaAs(001) wafer. It is measured with  $\theta_A = 0^\circ$  and  $\alpha - \beta = 90^\circ$  in Fig. 3. The negative sign is introduced using the

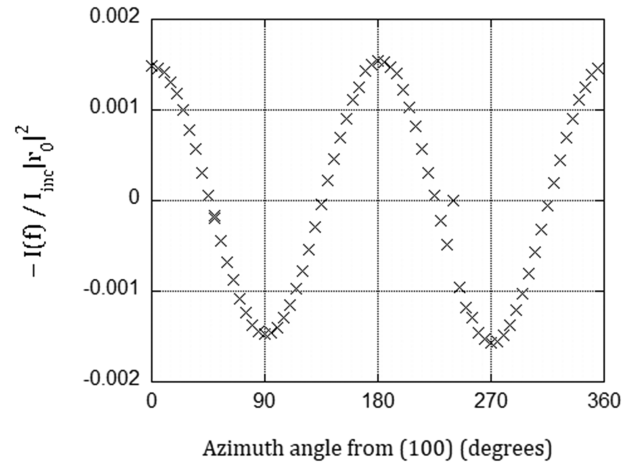
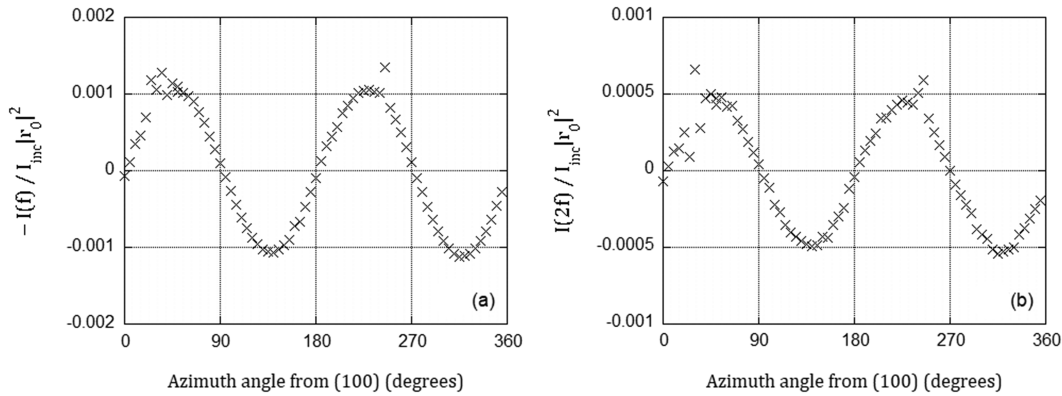


FIG. 4. The first harmonic in the reflected intensity divided by the total reflected intensity,  $-I(f)/I_{inc}|r_0|^2$ , vs azimuth angle  $\phi$  about the  $z$  axis (pointing into the sample).



**FIG. 5.** (a) The first harmonic in the reflected intensity divided by the total reflected intensity,  $-I(f)/I_{inc}|r_0|^2$ , vs azimuth angle  $\phi$ . (b) The second harmonic divided by the total reflected intensity,  $I(2f)/I_{inc}|r_0|^2$ , vs azimuth angle  $\phi$ . Both measurements are done with the scheme shown in Fig. 3.

phase setting of the lock-in amplifier. The signal varies as  $\cos 2\phi$ , as expected from Eq. (15) or the off-diagonal element of the reflection matrix,  $\Delta r_{ps} = -a \cos 2\phi$ . With  $J_1(\pi/2) = 0.56$ , I find  $|a/r_0| = 1.4 \times 10^{-3}$ . Since  $a/r_0 = (-i)d_{14}(2\pi/\lambda)/(\epsilon_2 - 1) \cong (-i)d_{14}(2\pi/\lambda)/14$  and  $\lambda = 0.633\mu\text{m}$ , I arrive at  $|d_{14}| = 2.0 \times 10^{-9}$  m. This makes  $|d_{14}^{(2)}| \cong 1.0 \times 10^{-9}$  m/V at  $\lambda = 0.633\mu\text{m}$ . It is 2.5 times larger than  $|d_{14}^{(2)}| \cong 0.37 \times 10^{-9}$  m/V at  $\lambda = 10\mu\text{m}$  for GaAs.<sup>3,8</sup>

### B. Measuring $Im\{a/r_0\}$

In Fig. 5(a), I show  $-I(f)/I_{inc}|r_0|^2$  vs azimuth angle  $\phi$  from the GaAs(001) wafer. It is measured with  $\theta_A = -45^\circ$  and  $\alpha = 0^\circ$  in Fig. 3. The signal varies as  $\sin 2\phi$ , as expected from Eq. (16) or the correction to the diagonal element of the reflection matrix,  $\Delta r_{pp} = -a \sin 2\phi$ . Again with  $J_1(\pi/2) = 0.56$ , I find  $Im\{a/r_0\} = -0.98 \times 10^{-3}$ .

In Figure 5(b), I show  $I(2f)/I_{inc}|r_0|^2$  vs azimuth angle  $\phi$  from the GaAs(001) wafer measured with  $\theta_A = -45^\circ$  and  $\alpha = 90^\circ$  in Fig. 3. It varies as  $\sin 2\phi$  as expected from Eq. (19). With  $J_2(\pi/2) = 0.25$ , I arrive at  $Im\{a/r_n\} = -0.91 \times 10^{-3}$ .

### C. Measuring $Re\{a/r_0\}$

In Figs. 6(a) and 6(b), I display  $-I(f)/2I_{inc}|r_0|^2$  and  $I(2f)/2I_{inc}|r_0|^2$  as functions of azimuth  $\phi$  using the scheme in Fig. 3 without the analyzer. Both vary as  $\cos 2\phi$ , in agreement with Eqs. (20) and (21). I further deduce  $|Re\{a/r_0\}| = 0.88 \times 10^{-3}$  using Eqs. (20) and (21). From values of  $Im\{a/r_0\}$  and  $|Re\{a/r_0\}|$ , I find  $\sqrt{Re\{a/r_0\}^2 + Im\{a/r_0\}^2} = 1.33 \times 10^{-3}$ , in good agreement with the separately measured  $|a/r_0| = 1.4 \times 10^{-3}$ . It shows that the normal-incidence reflectivity difference illustrated in Fig. 3 is a most effective scheme as it independently measures  $Im\{a/r_0\}$ ,  $Re\{a/r_0\}$ , and  $|a/r_0|$ .

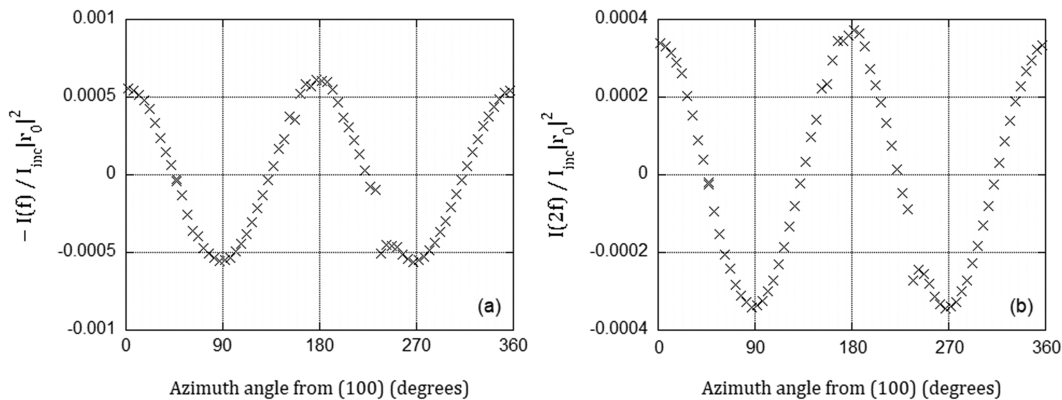


**FIG. 6.** (a) The first harmonic signal in the reflected intensity divided by the total reflected intensity,  $-I(f)/I_{inc}|r_0|^2$ , vs azimuth angle  $\phi$ . (b) The second harmonic signal in the reflected intensity divided by the total reflected intensity,  $I(2f)/I_{inc}|r_0|^2$ , vs azimuth angle  $\phi$ . Both measurements are done using the setup shown in Fig. 3 without the analyzer.

Since  $r_0$  is known, the quadrupole susceptibility tensor element as a complex number is easily determined.

As I illustrated here, normal-incidence reflectivity difference detection (NI-RD) involving polarization modulation can be configured to suppress or even eliminate the effect of the leading order dielectric response while revealing much weaker effects from the electric quadrupole process. Figure 2 shows one realization of NI-RD in which the first and second harmonics of modulation frequency in the reflected beam intensity are directly proportional to corrections to the diagonal and off-diagonal reflection matrix caused by the linear quadrupole response. Its only deficiency is that it only detects real parts of the corrections. Figure 3 shows a more versatile realization of NI-RD in which the first and second harmonics of modulation frequency can be made directly proportional to absolute values or imaginary parts or real parts of the corrections. As a result, it can be used to fully characterize the quadrupole susceptibility tensor element, as long as azimuth-dependent corrections are non-vanishing at normal incidence. This applies to crystals with cubic symmetry and uniaxial crystals.

The convenience of optical reflection measurement comes with a limitation. That is, the signal is mostly from a region near the surface having an effective thickness in the order of optical wavelength or less.<sup>9,10</sup> This makes the effects on optical reflection from processes such as linear quadrupole response and magneto-optic response small and difficult to observe in many cases. Most nonlinear optical crystals have much smaller second-order nonlinear susceptibilities  $\chi_D^{(2)}$  when compared with that of GaAs. Electric quadrupole susceptibility tensors  $\chi_Q^{(1)}$  in these materials are expected to be small accordingly. What limits the detection sensitivity is the inhomogeneity of a real crystalline sample and the effect from the surface layer. Over the illuminated area, linear electric dipole responses in the surface layer and even inside the bulk have residual anisotropy as a result of crystal growth and preparation. They yield an anisotropic background that superimposes on the EQ response. Experimentally, these residual anisotropic effects from the electric dipole response can be eliminated by performing microscopic measurements on a single domain of the sample.<sup>7</sup> Furthermore, by placing the sample should be inside an ultrahigh vacuum, the anisotropy originated from the surface layer can be removed with suitable surface treatments.

Alternatively, one may use transmission difference detection schemes similar to Fig. 3. Transmission measurements increase the effect of  $\vec{\epsilon}$  by the ratio of the sample thickness to the optical wavelength. For example, the Faraday rotation (in transmission) is known to be much larger than Kerr rotation (in reflection) from a magnetic material.<sup>11–13</sup> This is because the Faraday effect is accumulative over a much larger distance. For the same reason, optical second-harmonic reflection from a nonlinear crystal is much weaker than optical second-harmonic transmission in the same crystal under the phase-matched condition.<sup>3</sup> For transparent materials, a weak dielectric response such as magneto-optic effect and electric quadrupole effect can produce a large effect on transmission due to enhanced “interaction” lengths.

## ACKNOWLEDGMENTS

The author acknowledges the support in the form of a Visiting Lecture Professorship and a Fudan Fellow from Fudan University.

## APPENDIX: JONES MATRIX CALCULATION FOR NORMAL-INCIDENCE REFLECTIVITY DIFFERENCE (NI-RD) DETECTION

For completeness, I here describe key elements of Jones matrix calculation that lead to Eqs. (10)–(12) and Eqs. (20) and (21). It suffices to list the initial Jones vector and Jones matrices of the optical elements right before the photo-detector (PD). The intensity measured by using the photo-detector is the initial beam intensity  $I_{inc}$  before the photo-elastic modulator (PEM) multiplied by the sum of squares of the Jones vector components.

For NI-RD shown in Fig. 2, the initial beam is  $p$ -polarized and has a Jones vector,

$$\vec{E}_{inc} = \begin{pmatrix} 1 \\ 0 \end{pmatrix}. \quad (A1)$$

The Jones matrices for the PEM, phase shifter, and the bending mirror are as follows:

$$M_{PEM}(FA@45^\circ) = \frac{1}{2} \begin{pmatrix} 1 + e^{i\phi(t)} & 1 - e^{i\phi(t)} \\ 1 - e^{i\phi(t)} & 1 + e^{i\phi(t)} \end{pmatrix}, \quad (A2)$$

$$M_{PS}(\Delta_{PS}) = \begin{pmatrix} 1 & 0 \\ 0 & e^{i\Delta_{PS}} \end{pmatrix}, \quad (A3)$$

$$M_{mirror} = \begin{pmatrix} e^{i\Phi_p} & 0 \\ 0 & e^{i\Phi_s} \end{pmatrix}. \quad (A4)$$

The Jones matrix for the sample is the reflection matrix given by Eq. (10),

$$M_{sample} = R(\theta_{inc} = 0) = \begin{pmatrix} r_0 - a \sin 2\phi & -a \cos 2\phi \\ -a \cos 2\phi & r_0 + a \sin 2\phi \end{pmatrix}. \quad (A5)$$

The Jones vector before the photo-detector is given by

$$\vec{E}_{final} = \begin{pmatrix} p \\ q \end{pmatrix} = M_{sample} M_{mirror} M_{PS}(\Delta_{PS}) M_{PEM}(FA@45^\circ) \vec{E}_{inc}. \quad (A6)$$

The reflected beam intensity measured by using the photo-receiver is given by

$$I(t) = I_{inc}(p^2 + q^2). \quad (A7)$$

By only keeping terms in  $(p^2 + q^2)$  up to those that vary linearly with the small parameter  $a$  in the reflection matrix (A5), we arrive at the expression for the reflected beam intensity,

$$\begin{aligned} I(t) = & I_{inc}|r_0|^2 + 2 * I_{inc}|r_0|^2 * Re\{a/r_0\} * \cos 2\phi^* \sin \Phi(t) \\ & * \sin(\Phi_p - \Phi_p + \Delta_{ps}) - 2 * I_{inc}|r_0|^2 * Re\{a/r_0\} \\ & * * \sin 2\phi^* \cos \Phi(t). \end{aligned} \quad (A8)$$

Equations (10) and (11) are obtained from (A8) by setting  $\Phi_p - \Phi_p + \Delta_{ps} = 90^\circ$ , expanding  $\cos \Phi(t)$  and  $\sin \Phi(t)$ , and keeping the first and second harmonics.

For NI-RD shown in Fig. 3, the initial beam is linearly polarized with equal s-polarized and p-polarized components and has a Jones vector,

$$\tilde{E}_{inc} = \frac{1}{\sqrt{2}} \begin{pmatrix} 1 \\ 1 \end{pmatrix}. \quad (A9)$$

The Jones matrices for the PEM with its fast axis along the p-polarization and the analyzer after the sample are as follows:

$$M_{PEM}(FA@0^\circ) = \begin{pmatrix} 1 & 0 \\ 0 & e^{i\phi(t)} \end{pmatrix}, \quad (A10)$$

$$M_{PL}(TA@0^\circ) = \begin{pmatrix} \cos^2\theta_A & \cos\theta_A \sin\theta_A \\ \cos\theta_A \sin\theta_A & \sin^2\theta_A \end{pmatrix}. \quad (A11)$$

The Jones vector right before the photo-receiver is given by

$$\begin{aligned} \tilde{E}'_{final} = \begin{pmatrix} p' \\ q' \end{pmatrix} &= M_{PL}(TA@0^\circ) M_{sample} M_{mirror} M_{PS}(\Delta_{PS}) M_{PEM} \\ &\times (FA@0^\circ) \tilde{E}_{inc}. \end{aligned} \quad (A12)$$

The reflected beam intensity measured by using the photo-receiver is given by

$$I(t) = I_{inc}(p'^2 + q'^2). \quad (A13)$$

Again, by only keeping terms in  $(p'^2 + q'^2)$  up to those that vary linearly with the small parameter  $a$ , we arrive at Eq. (12) in the main text,

$$\begin{aligned} I(t) &= \frac{I_{inc}|r_0|^2}{2} + I_{inc}|r_0|^2 \sin\theta_A \cos\theta_A [\cos\Phi(t) \cos(\alpha - 2\gamma) \\ &+ \sin\Phi(t) \sin(\alpha - 2\gamma)] - I_{inc}|r_0|^2 \left| \frac{a}{r_0} \right| \cos 2\phi \\ &\times [\cos^2\theta_A \cos(\alpha - \beta - \Phi(t)) + \sin^2\theta_A \cos(\alpha + \beta - \Phi(t))]. \end{aligned} \quad (A14)$$

Here,  $\alpha = \Phi_p - \Phi_s - \Delta_{PS}$ , and  $\beta = \arg\{a/r_0\}$  is the phase of  $a/r_0$ .  $\gamma = -\text{Im}\{\Delta r_{pp}/r_0\} = \text{Im}\{a/r_0\} \sin 2\phi$ .

Finally, by removing the analyzer in Fig. 3, the Jones vector immediately before the photo-receiver is given by

$$\tilde{E}''_{final} = \begin{pmatrix} p'' \\ q' \end{pmatrix} = M_{sample} M_{mirror} M_{PS}(\Delta_{PS}) M_{PEM}(FA@0^\circ) \tilde{E}_{inc}. \quad (A15)$$

The reflected beam intensity measured by using the photo-receiver is given by

$$I(t) = I_{inc}(p''^2 + q'^2). \quad (A16)$$

Keeping terms in  $(p''^2 + q'^2)$  up to those that vary linearly with the small parameter  $a$ , we arrive at the following expression for the reflected intensity:

$$I(t) = I_{inc}|r_0|^2 - 2 * I_{inc}|r_0|^2 * \text{Re}\{a/r_0\} * \cos 2\phi^* \cos(\alpha - \Phi(t)). \quad (A17)$$

Again,  $\alpha = \Phi_p - \Phi_s - \Delta_{PS}$ . By keeping only the first and second harmonics in Eq. (A17), we obtain Eqs. (20) and (21).

## DATA AVAILABILITY

The data that support the findings of this study are available from the corresponding author upon reasonable request.

## REFERENCES

- E. Alder, "Nonlinear optical frequency polarization in a dielectric," *Phys. Rev.* **134**, A728 (1964).
- X. D. Zhu and H. Zhang, "Hidden linear optical response reveal crystalline symmetry," *Opt. Lett.* **45**, 2439 (2020).
- Y. R. Shen, *The Principles of Nonlinear Optics* (John Wiley & Sons, New York, 1984).
- H. W. K. Tom, T. F. Heinz, and Y. R. Shen, "Second-harmonic reflection from silicon surfaces and its relation to structural symmetry," *Phys. Rev. B* **51**, 1983 (1983).
- H. W. K. Tom and G. D. Aumiller, "Observation of rotational anisotropy in the second-harmonic generation from a metal surface," *Phys. Rev. B* **33**, 8818 (1986).
- D. L. Everitt, W. J. W. Miller, N. L. Abbott, and X. D. Zhu, "Evolution of a preferred orientation of polycrystalline grains in obliquely deposited gold films on an amorphous substrate," *Phys. Rev. B* **62**, R4833 (2000).
- L. Zhao, D. H. Torchinsky, H. Chu, V. Ivanov, R. Lifshitz, R. Flint, T. Qi, G. Cao, and D. Hsieh, "Evidence of an odd-parity hidden order in a spin-orbit coupled correlated iridate," *Nat. Phys.* **12**, 32 (2016).
- R. L. Sutherland, *Handbook of Nonlinear Optics*, 2nd ed. (Marcel Dekker, New York, 2003), pp. 296–316.
- X. D. Zhu, "Linear optical responses beyond the electric dipole process in materials—Perturbation effects on optical reflection," OSA-Continuum (submitted).
- T. F. Heinz, "Second-order nonlinear optical effects at surfaces and interfaces," in *Nonlinear Surface Electromagnetic Phenomena*, edited by H. E. Ponath and G. I. Stegeman (Elsevier Science Publisher, B.V., 1991), p. 353.
- W. Voigt, *Magneto- und Electro-Optik* (Teuner, Leipzig, 1908).
- Z. Q. Qiu and S. D. Bader, "Surface magneto-optic Kerr effects," *Rev. Sci. Instrum.* **71**, 1243 (2000).
- R. P. Hunt, "Magneto-optic scattering from thin solid films," *J. Appl. Phys.* **38**, 1652 (1967).